10 Particle Physics with CMS

C. Amsler, R. Kaufmann, H. Pruys, C. Regenfus, P. Riedler‡,
P. Robmann, T. Speer, and S. Steiner

in collaboration with:
ETH-Zürich, Paul Scherrer Institut (PSI), Universität Basel and the CMS Collaboration.

(CMS Collaboration)

‡ now at CERN, Geneva, Switzerland

10.1 Introduction

Our group is participating in the design and construction of the silicon pixel detectors for the CMS experiment at CERN's LHC, which is scheduled to start operations in spring 2006 at an energy of $\sqrt{s} = 14$ TeV. We shall concentrate on issues related to the heavy b and t quarks. The physics programme with CMS is focused on the Higgs boson(s) and on the supersymmetric (SUSY) particles, expected in the ~ 1 TeV mass range. The B physics programme is centered on the search and measurement of CP-violation through the decays $B^0_d \to J/\psi K_s$, $B^0_d \to \pi^+\pi^-$ and $B^0_s \to J/\psi\phi$, the measurement of B^0_s mixing, and searches for flavor changing neutral currents decays. The study of B-baryon decay and the spectroscopy of B hadrons could also be undertaken.

The identification of b-jets is crucial both to select signal events and to reject background events; b-jets will be used to identify top quarks, the standard model Higgs boson and SUSY particles. Due to the long lifetime of B mesons, b-jets can be identified by looking for tracks not pointing to the primary vertex (i.e. with large impact parameters). Trajectories have to be measured with a high precision that depends on the distance of the first detected point from the interaction vertex, and on the point resolution. It is thus crucial that the first detector layer be located as close as possible to the primary interaction vertex, bearing in mind the high radiation which the pixel detectors will have to withstand. The high rate requires a fine detector granularity and also developments using radiation hard technology.

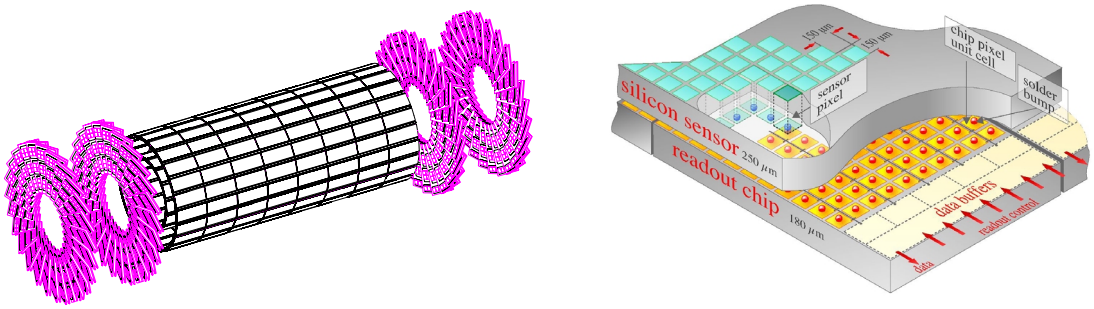

Figure 10.1: *a): Perspective view of the CMS pixel detector. b): schematic view of a pixel detector element. Each sensor pixel is connected via an indium solder bump to a pixel unit cell on the readout chip which amplifies the signal. The hit data are stored on the edge of the chip where they wait for trigger confirmation.*

The pixel detector envelope extends from 3.7 to 21 cm radially and from -50 to 50 cm in beam direction. The detector is made of three cylindrical layers, 53 cm long, with radii of 4, 7 and 11 cm (Fig. 10.1a). The layers contain some 3×10^7 silicon pixels. The pixel modules consist of thin, segmented sensor plates with highly integrated readout chips connected with

the indium bump bonding technique (see Fig. 10.1b). A sensor plate contains 53 × 52 pixels, each with a surface area of 150×150 μm^2. The analogue signals are read out to determine the coordinates more accurately, using charge sharing between adjacent pixels. A double column of pixels forms an independent readout unit controlled by a circuit sitting in the periphery. The chips are connected through bond wires to hybrid circuits, which collect the data signals and distribute the readout control and clock signals. Capton cables connected to the hybrids transmit the signals to and from the outer region of the pixel system frame which contains detector control chips and electro-optical converters for optical signal transmission.

We have worked on the design and test of the silicon sensors for the barrel detector [1]. Position resolutions and depletion depths were measured at CERN for various magnetic field configurations [2] and for detectors that had been irradiated with doses equivalent to several years of LHC operation. Full details can be found in previous annual reports, in several diploma works and in ref. [3, 4].

We are also designing and building the mechanical support and cooling structure for the pixel detector in the Institute's workshop, as well as the service tubes which will contain the electrical and cooling lines. All these projects are currently in the R & D phase. During last year most of our hardware efforts were devoted to the commissioning of the ATHENA experiment. We nevertheless studied various pixel designs and studied their performances before and after irradiation in the laboratory, and with a test beam at CERN. We also started to contribute towards simulation and reconstruction for the trackfinder software.

10.2 Test of irradiated pixel sensors

In 2000 we irradiated the pixel sensors ordered earlier from SINTEF (Norway) and CSEM (Neuchâtel). They consist of a 300 μm n-type silicon bulk with n^+ pixel implants. The p-n junction was made by implanting a p^+ layer on the sensor backside [5]. In the non-irradiated sensor the depletion zone grows from the p^+ side, but during irradiation, type inversion occurs and the depletion zone then grows from the pixel side. The prototypes from the two vendors were irradiated with 24 GeV/c protons from the CERN-PS and with 300 MeV/c pions at PSI. The devices were submitted to various charged particle fluxes, some reaching 6×10^{14} hadrons/cm^2, which corresponds to the accumulated dose of the innermost layer after several years of LHC operation.

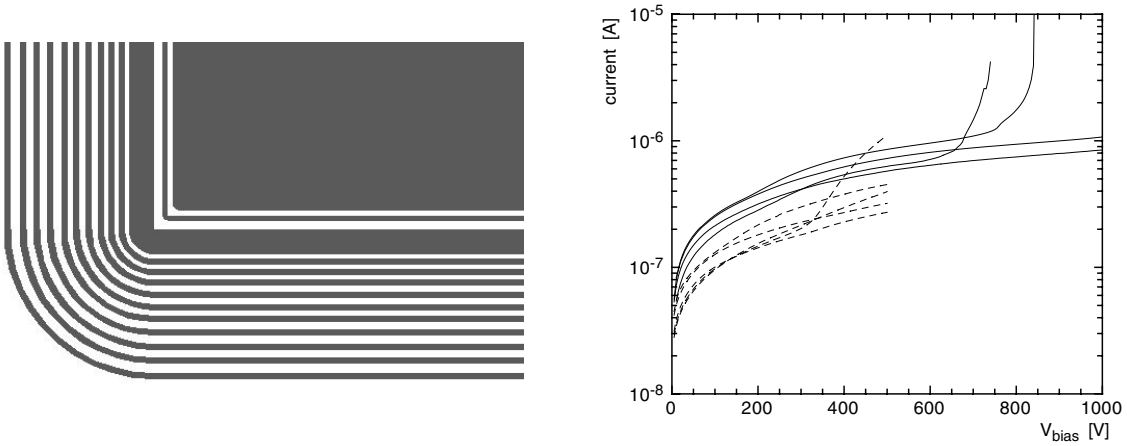

Figure 10.2: *Left: one of the various guard-ring designs. Right: leakage currents of irradiated diodes with different guard ring designs. Full curves: test up to 1 kV, dashed curved: test up to 500 V.*

10.2.1 Guard ring design

The bias voltage needed to guarantee a sufficient depletion depth increases with time due to the accumulation of radiation defects and the sensors will eventually have to withstand a bias voltage of several hundred volts. This requires an advanced guard ring structure around the sensor plate. Different structures have been designed, built and tested after irradiation. One of them is shown in Fig. 10.2 (left).

The leakage-currents of nine different diodes after irradiation with 6×10^{14} hadrons/cm^2 are plotted in Fig. 10.2 (right), as a function of bias voltage. The surface surrounded by the guard rings was between 1 and 4 mm^2. From the four devices that were tested up to 1 kV, two sustained 1000 V, whereas two broke down already at 700 V. The other devices were only tested up to 500 V, with only one performing unsatisfactorily below 500 V. In conclusion, a guard-ring structure of the type shown in Fig. 10.2 (left) is suitable for the harsh radiation environment at LHC.

10.2.2 Pixel design

Since the pixels consist of n^+ silicon in an n-type substrate they have to be insulated. This is normally done with a narrow p^+-ring around each pixel, called p-stop ring. When the detector is fully depleted the pixels are perfectly insulated against each other. However, a (hopefully small) fraction of pixels will fail, owing to the poor connection with the readout chip through the indium bump. The accumulation of charge on these pixels will lead to a local breakdown through the narrow gap to the read-out chip, generating a dead cluster around the faulty pixel. This can be avoided by reducing the resistance between the pixels, for instance with the atoll structure and small openings in the p-stop rings shown in Fig. 10.3 (left). The long paths through the maze provide enough resistance, yet allow the accumulated charge to flow in a controlled way. Simulations show that the inter-pixel resistance should be at least a few MΩ in order not to influence the fast signal-charge collection.

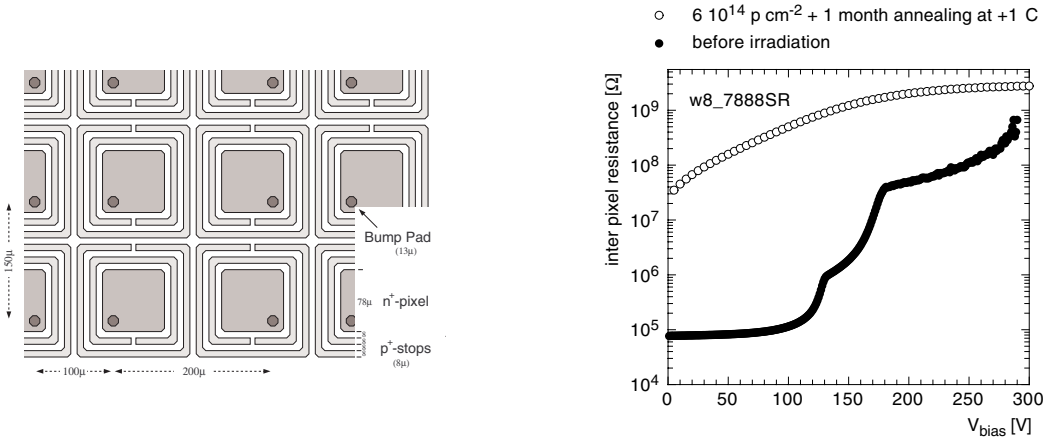

Figure 10.3: *Left: Pixel layout with atoll-like open double p-stop rings. Right: Interpixel resistance as a function of bias voltage, before and after irradiation, for a device with only one open p-stop ring.*

Figure 10.3 (right) shows the resistance between one pixel and all of its neighbours for a device with only one open p-stop ring, before and after irradiation. The full depletion voltage of the non-irradiated device was 140 V. The quite different shape of the irradiated curve is due the bulk type-inversion. The resistance after irradiation has increased by several

orders of magnitude and is in the range of $\sim 1\,\mathrm{G}\Omega$. Figure 10.4 shows the behaviour of the inter-pixel resistance as a function of fluence (time integrated hadron flux). The maximal fluence of $6 \times 10^{14}\,\mathrm{cm}^{-2}$ corresponds roughly to a dose of 2×10^{5} Gy.

The inter-pixel resistance decreases at low fluencies but increases dramatically at higher doses. The low fluence behaviour could be explained by the build-up of an electron accumulation layer at the surface on the pixel-side. At higher doses the influence of surface defects (reduced surface mobility, interface traps, etc) over-compensates for the effect of the accumulated charge and lead again to an increase in resistance.

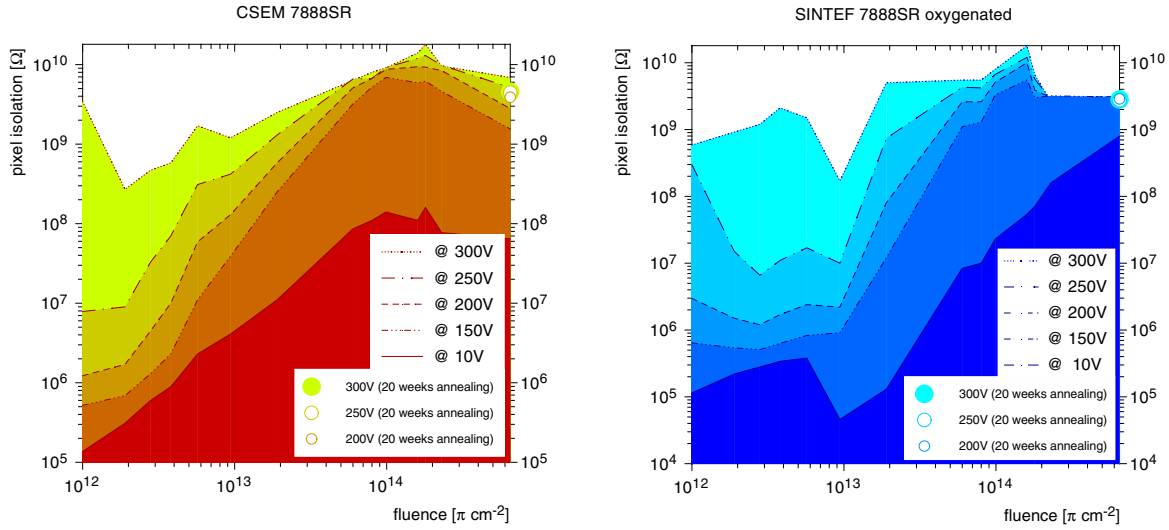

Figure 10.4: *Inter-pixel resistance as a function of pion fluence for a typical CSEM device (left) and an oxygenated SINTEF device (right), both with one open p-stop ring.*

10.2.3 Oxygenated silicon pixels

Recently, the CERN RD48 collaboration (also known as ROSE-collaboration) demonstrated that a high oxygen concentration in the silicon bulk can increase the radiation hardness of detectors. In fact, it reduces the so-called β factor, which denotes the introduction rate of negative space charge after type inversion [6]. In Fig. 10.4 there is no dramatic difference between the high dose inter-pixel resistances of a CSEM and an oxygenated SINTEF device, and therefore oxygenation does not influence significantly the surface defects. However, the smaller β factor is still useful, as it reduces the full depletion voltage $V(FD)$ after irradiation. Several diodes were irradiated with pions at PSI to measure $V(FD)$ and the doping concentration N_{eff}. After a fluence of $6 \times 10^{14}\,\pi\ \mathrm{cm}^{-2}$, $V(FD)$ was about 190 V for the oxygenated device, which corresponds to N_{eff} =2.8 $\times 10^{12}\,\mathrm{cm}^{-3}$. However, $V(FD)$ was much higher for the non-oxygenated device ($> 400\,\mathrm{V}$), leading to $N_{eff} > 6 \times 10^{12}\,\mathrm{cm}^{-3}$.

10.2.4 Beam tests

In summer 2000 a preliminary readout chip (DM_PSI38), designed by our PSI colleagues in radiation hard DMILL technology, and fully equipped with bump bonded sensors, was submitted to a beam test at CERN. We used the 220 GeV/c pion beam H2 produced with the SPS proton beam. Figure 10.5 shows a remarkable Landau pulse height distribution for events from one pixel only. Since the chip was used in self-triggering mode, the noise peak is cut off.

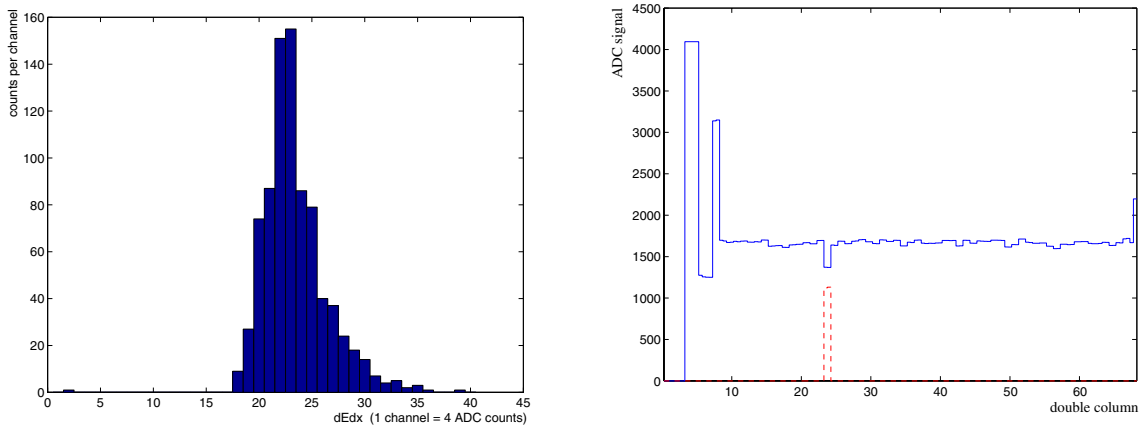

Figure 10.5: *Left: Pulse height distribution from one pixel only, taken with 220 GeV/c pions. Right: Output signal distribution from the DM_PSI30 chip showing a signal from the bump bonded pixel. The whole double column was read out after a pixel hit (see text).*

A single event registered with our sensors by the DM_PSI30 chip is shown in Fig. 10.5 (right). The continuous line shows the contents of the analogue cells of one double column. The first analogue signals (up to count 8 on the horizontal axis) consist of time stamps and column address. The analogue values of the 60 pixels of one double column are displayed above x=9. The dashed signal marks a pixel with analogue signal above threshold. At $x = 23$ a clear analogue signal from pixel 14 can be seen, confirmed by its digital output.

To optimize the atoll design and in an attempt to increase the breakdown voltage after irradiation, we will design and order a last batch of pixel sensors with various p-stop geometries, before a final decision is taken in 2002. One possible way to remove the accumulated charge would be to implant a uniform p-layer on the surface (p-spray technique). On the other hand, we have shown that the current layout is already adequate for several years of LHC operation.

10.3 Tracking at CMS: the combinatorial forward Kalman filter

With the high luminosity of the LHC, the challenge of track reconstruction is to reliably find tracks in a high density environment, where low luminosity events will feature around 5000 hits and high luminosity events ten times more. With this high number of hits, combinatorial problems can be severe, and the challenge is to find for each track the correct combination of hits, while limiting the number of spurious combinations leading to ghost tracks in a reasonable amount of time.

Tracks usually leave between 8 and 15 hits in the tracker (pixel and silicon detectors), according to their rapidity. However, some of these hits may be missed, due for example to detector inefficiencies. The track reconstruction algorithm has therefore to exclude bad hits, for example background hits near the tracks, and accommodate layers without hits.

Several algorithms were studied for CMS in the past [3]. In the new object-oriented reconstruction framework (ORCA), the first method to be pursued is the combinatorial forward Kalman filter. The Kalman filter was extensively used in high energy physics experiments [7]. In the combinatorial Kalman filter only one track is reconstructed at a time, starting from an initial trajectory. It is a recursive procedure to estimate the track parameters from a set of reconstructed hits, taking into account the random perturbation of the particle trajectory due to the material traversed. The filter proceeds iteratively from the innermost tracker

layer towards the outer layers, starting from a coarse estimate of the track parameters and including the information of the successive detection layers, one by one.

The first step is the construction of the initial trajectories, called *seeds*. These are composed of two hits in two pixel layers and the beam crossing region. In the present algorithm, any combination of two pixel layers are used, and seeds are constructed for every pair of hits pointing to the the beam crossing region and a specified minimum transverse momentum.

In the next step, track candidates are grown from each seed: the initial seed trajectory is extrapolated to the next layer, according to the expected motion in the magnetic field, accounting for multiple scattering and energy loss in the traversed material. On the new layer several hits may be compatible with the extrapolated trajectory and thus several trajectories are constructed, each time with a different hit. An additional trajectory candidate is created, in which no measured hit is used, to account for tracks with no hit on that particular layer. All trajectory candidates are then grown in turn to the next layer, and the procedure is repeated until the outer layer of the tracker is reached. To avoid a bias, the trajectory candidates are grown in parallel and, to limit the number of combinations, only the candidates with the best χ^2 are kept. Each seed usually leads to a large number of mutually exclusive trajectories which are partly composed of the same hits. A subset of compatible candidates, based on the number of hits shared and the track qualities, is therefore selected to resolve hit assignment ambiguities.

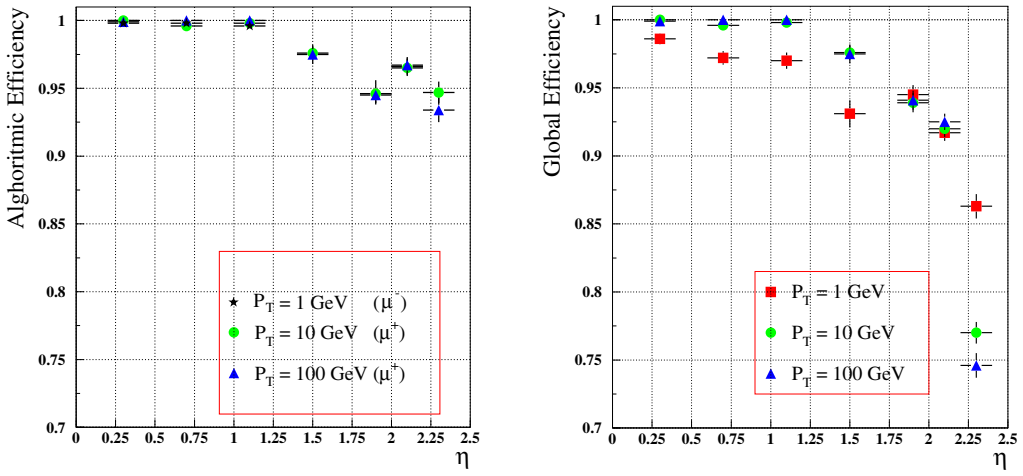

Figure 10.6: *Algorithmic (left) and global (right) track reconstruction efficiencies in single muon events, as a function of pseudo-rapidity* η.

Currently, a reconstructed track is required to have a minimum of 8 hits, with a hit missing in at most one layer. Two definitions are used for the track reconstruction efficiency. The *algorithmic* efficiency corresponds to tracks which have at least 8 hits in the tracker, among them at least 2 in the pixel detector. The *global* efficiency is the reconstruction efficiency for all tracks. In addition to the algorithmic efficiency, it also includes the acceptance, hit efficiency and any other factor influencing reconstruction. It mainly differs from the algorithmic efficiency in the forward region due to the loss of coverage.

The algorithmic and global track reconstruction efficiencies for single muon events are shown in Fig. 10.6. In the central region ($|\eta| < 1$) the algorithmic efficiency is nearly 100%. In the $|\eta| > 1$ region, the current algorithmic efficiencies of all samples are between 92% and

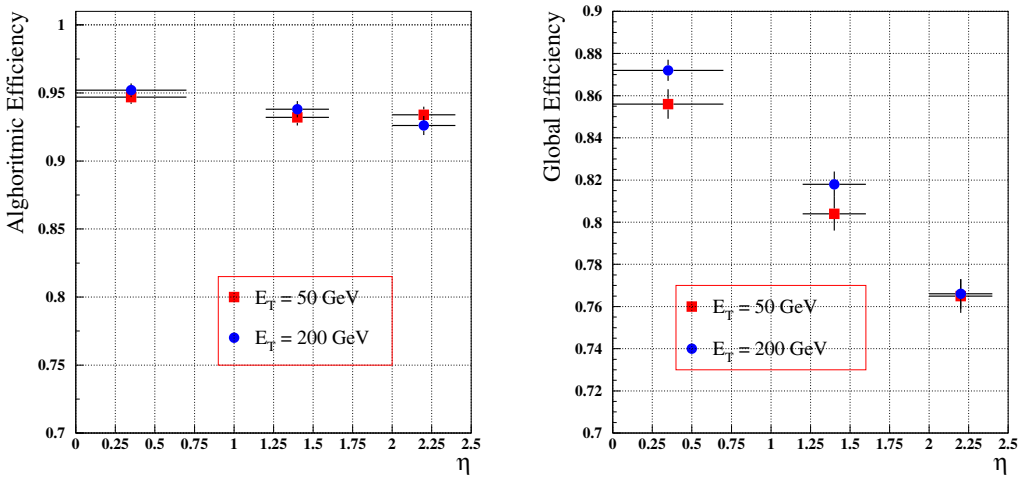

Figure 10.7: *Algorithmic (left) and global (right) track reconstruction efficiencies in $b\bar{b}$ jet events.*

97%. This somewhat low efficiency has been traced to shortcomings in the simulation.

The algorithmic and global track reconstruction efficiencies for $b\bar{b}$ jet events are shown in Fig. 10.7. The pseudo-rapidity bins correspond to the axis of the jets, and not to that of individual tracks.

Since no inefficiency related to the algorithm itself was found, the present effort is on improving the speed of the reconstruction (seed and trajectory building). At full luminosity, the large number of hits in the pixel layers leads to a very large number of seeds which do not grow into real tracks. Methods to reject spurious combinations as quickly as possible are being studied.

References

[1] R. Kaufmann, PhD thesis, in preparation

[2] V. Dubacher, Diplomarbeit, Universität Zürich (1996); R. Kaufmann, Diplomarbeit, Universität Zürich (1997); M. Glättli, Diplomarbeit, Universität Zürich (1998)

[3] Technical Design Report of the CMS Tracker, CERN/LHCC 98-6 (1998)

[4] R. Kaufmann and B. Henrich, Proc. of the ENDEASD Workshop, Santorin (1999) and Nucl. Instr. and Methods in Phys. Research A (in print)

[5] G. Bolla, D. Bortoletto, C. Rott, A. Roy, S. Kwan, C. Chien, H. Cho, B. Gobbi, R. Horisberger, K. Gabathuler, R. Kaufmann: Design and Test of Pixel Sensors for the CMS Experiment, Nucl. Instr. and Methods in Phys. Research A (in print)

[6] M. Moll, E. Fretwurst, G. Lindström (ROSE Collaboration), Nucl. Instr. Meth. in Phys, Res. A 439 (2000) 282

[7] R. Frühwirth, Nucl. Instr. Meth. in Phys. Research A 262 (1987) 444